Yasutaka Fujimoto* and Atsuo Kawamura**

Simulation of an Autonomous Biped Walking Robot Including Environmental Force Interaction

This autonomous biped walking control system is based on reactive force interaction at the foothold. The precise 3D dynamic simulation presented includes: 1) a posture controller which accommodates the physical constraints of the reactive force/torque on the foot with quadratic programming. 2) a real-time COM (center of mass) tracking controller for foot placement, with a discrete inverted pendulum model. 3) a 3D dynamic simulation scheme with precise contact with the environment. The proposed approach realizes robust biped locomotion because environmental interaction is directly controlled. The proposed method is applied to a 20 axes simulation model, and stable biped locomotion with velocity of 0.25 m/sec and a stepping time of 0.5 sec/step is realized.

A number of biped walking systems have been proposed in previous works[1]-[12]. Since the reactive force and torque on the foothold depend on its complicated characteristics, the relation between the input torque of the actuator and the reactive force and torque is hard to solve. Thus conventional control systems calculate trajectories of joint angle or joint torque so as to approximately satisfy the stable contact condition[1]-[3]. This approximation, however, does not yield walking robustness. The whole dynamic equation of the robot and the contact condition is considered to generate joints references in [3], but this is off-line type planning due to the complexity of dynamics of the biped robot.

*Department of System Design Engineering, Keio University, Kohoku-ku, Yokohama 223-8522 Japan. ** Department of Electrical and Computer Engineering, Yokohama National University, Hodogaya-ku, Yokohama 240-8501 Japan. Part of this research is subsidized by the Scientific Research Fund of the Ministry of Education.

To improve walking robustness, we propose a new hierarchical control system based on the reactive force control on the foothold and the force distribution system, in which the physical constraints of the contact force on the foothold are precisely considered. With a new foot placement algorithm, on-line controlled autonomous biped locomotion is realized. Also, a precise 3D dynamic simulator with environmental interaction is proposed to investigate the control scheme.

MODELING

A legged robot is modeled as a free-fall manipulator which has no fixed-point, but has interaction with the ground. The dynamics of a free-falling manipulator are formulated

 1070-9932/98/$10.00©1998 IEEE

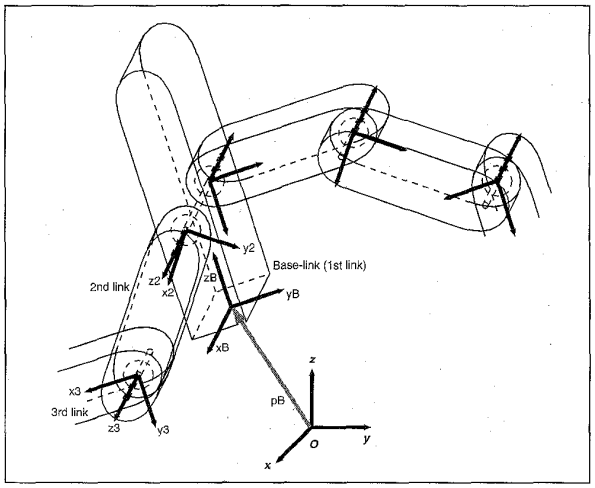

Figure 1. Representation of Link-fixed Coordinates.

by introducing the variables representing position and attitude of a *base-link*. Let generalized coordinates $\boldsymbol{x}$, generalized velocities u, and generalized forces $\boldsymbol{u}$ be

$$\boldsymbol{x}^T = \left[\boldsymbol{p}_B^T, \boldsymbol{A}_B^T, \theta^T\right] \in R^3 \times SO(3) \times R^N \tag{1}$$

$$\upsilon^T = \left[\upsilon_B^T, \omega_B^T, \omega^T\right] \in R^3 \times R^3 \times R^N \tag{2}$$

$$\boldsymbol{u}^T = \left[\boldsymbol{f}_B^T, \boldsymbol{n}_B^T, \tau^T\right] \in R^3 \times R^3 \times R^N \tag{3}$$

where

p_B : 3×1 vector specifying base-link position
A_B : 3×3 matrix specifying base-link attitude
θ : $N \times 1$ vector specifying joint angle
υ_B : 3×1 vector specifying base-link velocity
ω_B : 3×1 vector specifying angular velocity of base-link
ω : $N \times 1$ vector specifying joint angular velocity
f_B : 3×1 force vector generated in base-link
n_B : 3×1 torque vector generated in base-link
τ : $N \times 1$ torque vector generated by actuator
N : number of joints of robot

A_B is the direction matrix of the inertial base-link-fixed axes relative to the ground-fixed axes (see Figure 1, $A_B = [x_B, y_B, z_B]$.) The attitude A_B moves in the Lie group $SO(3)$.

The equations of motion of the robot become:

$$\dot{p}_B = \upsilon_B \tag{4}$$

$$\dot{A}_B = \omega_B \times A_B \tag{5}$$

$$\dot{\theta} = \omega \tag{6}$$

and

$$H(x)\dot{\upsilon} + C(x, \upsilon)\upsilon + g(x) = u + u_E \tag{7}$$

where

$H(x)$: $(N+6) \times (N+6)$ inertia matrix
$C(x, \upsilon)$: $(N+6) \times (N+6)$ matrix specifying centrifugal and Coriolis effects
$g(x)$: $(N+6) \times 1$ vector specifying gravity effect
u_E : $(N+6) \times 1$ vector specifying generalized forces generated by external forces

CONTROL ALGORITHM

To control a legged robot (Eqs. (4)-(7)), we must consider physical constraints on the foothold directly or indirectly. We propose a hierarchical control system with a direct and real-time method, which realizes robust contact of the foothold and the stable biped locomotion. Figure 2 shows the proposed hierarchical system. The lower layer consists of a workspace position controller and a robust reactive force controller.

Posture Controller

In a case of a biped robot, u_E, the external force on the generalized coordinates, is expressed as follows.

$$u_E = \begin{bmatrix} \boldsymbol{I}_3 & 0 \\ [\boldsymbol{x}_R \times] & \boldsymbol{I}_3 \\ \boldsymbol{J}_{R1}^T & \boldsymbol{J}_{R2}^T \end{bmatrix} \begin{bmatrix} \boldsymbol{f}_R \\ \boldsymbol{n}_R \end{bmatrix} + \begin{bmatrix} \boldsymbol{I}_3 & 0 \\ [\boldsymbol{x}_L \times] & \boldsymbol{I}_3 \\ \boldsymbol{J}_{L1}^T & \boldsymbol{J}_{L2}^T \end{bmatrix} \begin{bmatrix} \boldsymbol{f}_L \\ \boldsymbol{n}_L \end{bmatrix} \tag{8}$$

where

f_R, f_L : 3×1 vector of reactive force at the center of right or left foot
n_R, n_L : 3×1 vector of reactive torque at the center of right or left foot
J_{Ri}, J_{Li} : $3 \times N$ Jacobian matrix of right or left foot
x_R, x_L : 3×1 position vector of the right or left foot with respect to the origin of p_B

Here, $[a \times]$ denotes a matrix representing a cross product, and I_n denotes an $n \times n$ identity matrix.

While there is no actuated control input for the position and the attitude of the body, i.e., f_B=n_B=0, we can still control them by using the reactive force and torque (f_R, f_L, n_R, n_L) as indirect control inputs. To use the reactive force and torque as indirect control inputs, hybrid position/force control is applied to each leg. If the leg is in the support phase, the force control is activated. Otherwise the position control becomes active. The workspace position control system consists of inertia fluctuation insensitive servo control[14] and inverse kinematics by the Newton method. The force controller is applied as the upper layer of the position controller[15] (see Figure 2).

Next the posture control system is applied as a supervisory control to the reactive force controller. The objective is to make the *center of mass* (COM) of the robot and the attitude of the body converge to their given reference trajectories. The parallel motion of the COM of the robot and the rotational motion of the body can be modeled from the first 6 rows of (7) and (8) as follows.

$$\tilde{H}\dot{\tilde{\upsilon}} + \tilde{b} = \tilde{u}_E \tag{9}$$

$$\tilde{\boldsymbol{u}}_E = \tilde{\boldsymbol{K}}\boldsymbol{f}_A \tag{10}$$

and

$$\tilde{\boldsymbol{x}}^T = \left[\boldsymbol{p}_C^T \ \boldsymbol{A}_B^T\right] \tag{11}$$

$$\tilde{\upsilon}^T = \left[\upsilon_C^T \ \omega_B^T\right] \tag{12}$$

$$\boldsymbol{f}_A^T = \left[\boldsymbol{f}_R^T \ \boldsymbol{n}_R^T \ \boldsymbol{f}_L^T \ \boldsymbol{n}_L^T\right] \tag{13}$$

$$\tilde{\boldsymbol{K}} = \begin{bmatrix} \boldsymbol{I}_3 & 0 & \boldsymbol{I}_3 & 0 \\ [\boldsymbol{x}_R\times] & \boldsymbol{I}_3 & [\boldsymbol{x}_L\times] & \boldsymbol{I}_3 \end{bmatrix} \tag{14}$$

$$\dot{\boldsymbol{p}}_C = \upsilon_C \tag{15}$$

where

$\tilde{H}$: 6×6 inertia matrix
$\tilde{b}$: 6×1 vector specifying gravity effect and non-linear terms
$\tilde{u}_E$: 6×1 vector specifying external force at COM and external torque around body
p_C : 3×1 vector specifying COM of the robot

The ideal external force input $\tilde{u}_E^*$ at the COM of the robot and around the body is determined by the state feedback.

$$\tilde{\boldsymbol{u}}_E^* = \tilde{\boldsymbol{H}}_n\left[\boldsymbol{K}_p\left(\tilde{\boldsymbol{x}}_{ref}-\tilde{\boldsymbol{x}}\right)+\boldsymbol{K}_d\left(\dot{\tilde{\boldsymbol{x}}}_{ref}-\dot{\tilde{\boldsymbol{x}}}\right)+\ddot{\tilde{\boldsymbol{x}}}_{ref}\right]+\tilde{\boldsymbol{b}}_n \tag{16}$$

where

$\tilde{H}_n$: 6×6 diagonal matrix specifying nominal inertia
$\tilde{b}_n$: 6×1 constant vector specifying non-linear terms, gravity effect, and non-diagonal inertial force

and K_p, K_d represent gain matrices. The posture reference $\tilde{x}_{ref}$ is generated by linearized inverted pendulum models[16].

The contact force and torque are, however, physically limited to the repulsive condition, the friction condition, and *zero moment point* (ZMP) condition. Thus the ideal force $\tilde{u}_E^*$ is not always realized by the reactive force/torque f_A. We need to consider the following physical conditions. Let $f_R^T = [f_{Rx}\ f_{Ry}\ f_{Rz}]$, $n_R^T = [n_{Rx}\ n_{Ry}\ n_{Rz}]$, $f_L^T = [f_{Lx}\ f_{Ly}\ f_{Lz}]$, and $n_L^T = [n_{Lx}\ n_{Ly}\ n_{Lz}]$. The normal component of the reactive force on the ground plane is not attractive but repulsive, which yields the following non-negative conditions.

$$f_{Rz}\geq 0, \quad f_{Lz}\geq 0 \tag{17}$$

The friction force, i.e., the tangent component of the reactive force on the ground plane always exists within the friction cone.

$$\sqrt{f_{Rx}^2+f_{Ry}^2}\leq \mu f_{Rz} \quad \sqrt{f_{Lz}^2+f_{Ly}^2}\leq \mu f_{Lz} \tag{18}$$

$$|n_{Rz}|\leq \mu' f_{Rz} \quad |n_{Lz}|\leq \mu' f_{Lz} \tag{19}$$

where μ and μ' denote friction coefficients. It is possible to break out slips at the contact points when the equality in Eq.(18)-(19) is realized.

The tangent component of the reactive torque at the center of the foot on the ground plane is also limited due to the finiteness of the contact area.

$$|n_{Rx}|\leq d_y f_{Rz} \quad |n_{Lx}|\leq d_y f_{Lz} \tag{20}$$

$$|n_{Ry}|\leq d_x f_{Rz} \quad |n_{Ly}|\leq d_x f_{Lz} \tag{21}$$

where d_x and d_y denote half of the length and width of the foot, respectively. Eq.(20)-(21) are equivalent to the ZMP conditions.

Due to the physical limitations (Eq.(17)-(21)), the ideal force input $\tilde{u}_E^*$ by (16) cannot always be realized by the reactive force and torque f_A. Thus the following performance indices are introduced, which should be minimized under the limitations.

$$J_{main} = \frac{1}{2}\left(\boldsymbol{u}_E-\boldsymbol{u}_E^*\right)^T\boldsymbol{C}_1\left(\boldsymbol{u}_E-\boldsymbol{u}_E^*\right) \tag{22}$$

$$J_{sub} = \frac{1}{2}\boldsymbol{u}_E^T\boldsymbol{C}_2\boldsymbol{u}_E \tag{23}$$

The index J_{main} corresponds to the square error between the ideal force and torque and the realizable ones. The index J_{sub} corresponds to the square error between the force/torque of the left foot and those of the right. The reactive force and torque input f_A is determined by the quadratic programming, which minimizes the performance index under the linearized constraints of Eqs.(17)-(21).

$$\min_{f_A} \quad J_{main}+\varepsilon J_{sub} \tag{24}$$

$$\text{subject to} \quad \boldsymbol{A}\boldsymbol{f}_A\leq \boldsymbol{b} \tag{25}$$

where

$$\boldsymbol{C}_1 = \mathrm{diag}\{w_1,w_2,w_3,w_4,w_5,w_6\} \tag{26}$$

$$C_2 = \begin{bmatrix} I_6 & -I_6 \\ -I_6 & I_6 \end{bmatrix} \tag{27}$$

$$A = \begin{bmatrix} A' & 0 \\ 0 & A' \end{bmatrix} \tag{28}$$

$$A' = \begin{bmatrix} 1 & 0 & -\mu & 0 & 0 & 0 \\ -1 & 0 & -\mu & 0 & 0 & 0 \\ 0 & 1 & -\mu & 0 & 0 & 0 \\ 0 & -1 & -\mu & 0 & 0 & 0 \\ 0 & 0 & 1 & 0 & 0 & 0 \\ 0 & 0 & -1 & 0 & 0 & 0 \\ 0 & 0 & -d_y & 1 & 0 & 0 \\ 0 & 0 & -d_y & -1 & 0 & 0 \\ 0 & 0 & -d_x & 0 & 1 & 0 \\ 0 & 0 & -d_x & 0 & -1 & 0 \\ 0 & 0 & -\mu' & 0 & 0 & 1 \\ 0 & 0 & -\mu' & 0 & 0 & -1 \end{bmatrix} \tag{29}$$

$$b^T = [b_R^T \quad b_L^T] \tag{30}$$

$$b_R^T = [0\ 0\ 0\ 0\ z_R\ 0\ 0\ 0\ 0\ 0\ 0\ 0] \tag{31}$$

$$b_L^T = [0\ 0\ 0\ 0\ z_L\ 0\ 0\ 0\ 0\ 0\ 0\ 0] \tag{32}$$

$$z_R = \begin{cases} any & \text{if right leg is in support phase} \\ 0 & \text{otherwise} \end{cases} \tag{33}$$

$$z_L = \begin{cases} any & \text{if left leg is in support phase} \\ 0 & \text{otherwise} \end{cases} \tag{34}$$

and ε is a small positive real number.

The main performance index J_{main} approaches the solution to the ideal force and torque u_c^* given by the state feedback. The sub performance index J_{sub} distributes the inner force and torque to both feet in balance. Because ε is very small, the sub performance index has almost no influence on the main performance index. The constrained Eq.(25) acts as a kind of a limiter in multi-input systems.

The optimization problem of Eqs.(24) and (25) is equivalent to the following quadratic programming problem.

$$\min_{f_A} \quad \frac{1}{2} f_A^T Q f_A - c_o^T f_A \tag{35}$$

$$\text{subject to} \quad A f_A \le b \tag{36}$$

where $Q = \tilde{K}^T C_1 \tilde{K} + \varepsilon C_2$ and $c_0 = \tilde{K}^T C_1 u_c^*$. The reactive force and torque reference can be obtained by solving these equations at each sampling period.

Free-leg Trajectory Planner

Using the posture controller with the environmental interaction mentioned above, the on-line type autonomous walking control system can be realized as follows.

The posture controller mentioned above stabilizes the robot in the single and double support phases but does not realize the global locomotion. In order to achieve stable walking, the foot must periodically land at an adequate point. In this section, the tracking control of the COM by planning the landing point of the foot is described.

The dynamics of the COM of the robot behave like an inverted pendulum with the posture controller, i.e., $\ddot{p}_{cx} = \omega^2(p_{cx} - p_{gx})$ in the sagittal plane and $\ddot{p}_{cy} = \omega^2(p_{cy} - p_{gy})$ in the lateral plane, where p_{gx} and p_{cy} denote the COM position in the sagittal plane and in the lateral plane, respectively. p_{gx} and p_{gy} denote the foot position of the support leg with respect to the origin of the world fixed coordinates in the sagittal plane and in the lateral plane, respectively. Digitizing the inverted pendulum with one step period T, we have the discrete time inverted pendulum of Eq. (37). (Here, only the equations in the sagittal plane are described. The

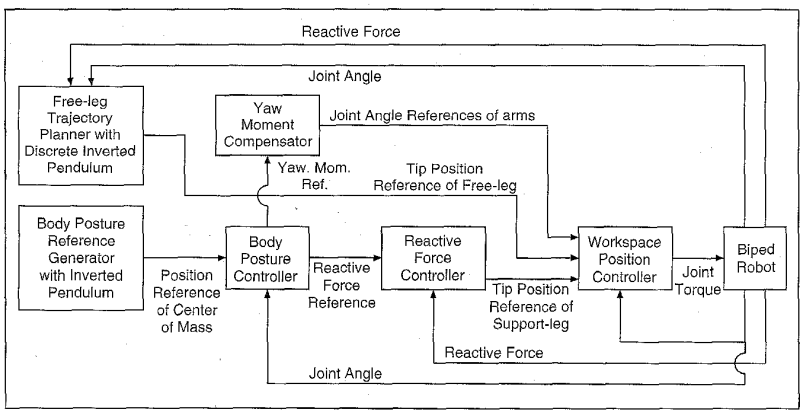

Figure 2. Biped Walking Control System.

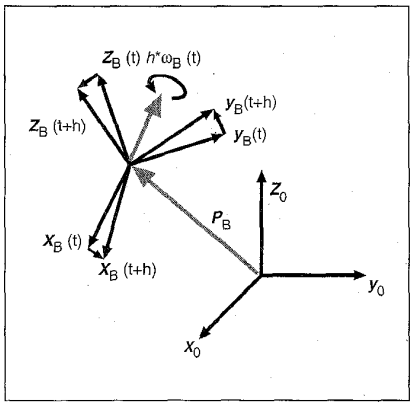

Figure 3. Rotation of Coordinates.

forms of the equations in the lateral plane are identical.)

$$\begin{bmatrix} p_{cx}(t+T) \\ \dot{p}_{cx}(t+T) \end{bmatrix} = \begin{bmatrix} c & \frac{s}{\omega} \\ \omega s & c \end{bmatrix} \begin{bmatrix} p_{cx}(t) \\ \dot{p}_{cx}(t) \end{bmatrix} + \begin{bmatrix} 1-c \\ -\omega s \end{bmatrix} p_{gx}(t) \tag{37}$$

where $c = \cosh\omega T$ and $s = \sinh\omega T$.

The movement of the free-leg must just begin at one step period in advance. Thus the augmented system, including one step period delay can be described as:

$$\begin{bmatrix} p_{cx}(t+T) \\ \dot{p}_{cx}(t+T) \\ p_{gx}(t+T) \end{bmatrix} = \begin{bmatrix} c & s/\omega & 1-c \\ \omega s & c & -\omega s \\ 0 & 0 & 0 \end{bmatrix} \begin{bmatrix} p_{cx}(t) \\ \dot{p}_{cx}(t) \\ p_{gx}(t) \end{bmatrix} + \begin{bmatrix} 0 \\ 0 \\ 1 \end{bmatrix} p_{gx}^{ref}(t) \tag{38}$$

The reference of the landing point $P_{gx}^{ref}(t)$, which sets the system characteristic polynomial $\phi(z)$ to $\phi(z) = z^3+\alpha_2 z^2+ \alpha_1 z + \alpha_0$ is obtained by the state feedback as follows.

$$\begin{aligned} p_{gx}^{ref}(t+T) = {} & f_0\left[p_{cx}(t) - p_{cx}^{cmd}(t)\right] \\ & + f_1\left[\dot{p}_{cx}(t) - \dot{p}_{cx}^{cmd}(t)\right] \\ & + f_2\left[p_{gx}(t) - p_{gx}^{cmd}(t)\right] \\ & + p_{gx}^{cmd}(t+1) \end{aligned} \tag{39}$$

where

$$f_0 = \frac{1-\alpha_0-\alpha_1+\alpha_2+2(1-\alpha_2)c-4c^2}{2(c-1)} \tag{40}$$

$$f_1 = \frac{1+\alpha_0-\alpha_1-\alpha_2-2(1+\alpha_2)c-4c^2}{2\omega s} \tag{41}$$

$$f_2 = \alpha_2 + 2c \tag{42}$$

p_{cx}^{cmd} denotes the reference trajectory of COM in the sagittal plane and p_{gx}^{cmd} denotes the offset of the landing points synchronizing the trajectory of COM in the sagittal plane.

The trajectory of the free-leg is given by connecting the next and previous landing points with a smooth function as follows.

$$p_{gx}^{ref}(t+m) = p_{gx}^{ref}(t-T) + \frac{1-\cos\pi m}{2}\left[p_{gx}^{ref}(t+T) - p_{gx}^{ref}(t-T)\right] \tag{43}$$

and the height of free-leg is also given by

$$p_{gz}^{ref}(t+m) = h^{ref}\frac{1-\cos 2\pi m}{2} \tag{44}$$

where $0 \le m \le T$.

The global system configuration is shown in Figure 2.

NEW SIMULATION SCHEME

We now describe a new simulation method for multi-degree-of-freedom mechanical systems with time dependent contact and Coulomb friction, such as a legged robot interacting with the ground, a satellite-mounted manipulator catching an object, etc. The proposed method is an extension of the open link manipulator simulation[20] and the contact simulation of rigid body mechanics[21]. The proposed simulation model is mathematically exact; thus this simulator enables the essential investigation for control algorithms of the mechanical systems.

Numerical Integration

It is easy to simulate the dynamic motion of a legged robot (Eqs.(4)-(7)) numerically by integrating $\dot{\upsilon}$ and υ on each time step after solving Eq.(7) for the acceleration $\dot{\upsilon}$ given x, υ, u, and u_E. In a case of the Euler integration, we have

$$P_B(t+h) = P_B(t) + h v_B(t) \tag{45}$$

$$A_B(t+h) = T(h\omega_B(t))A_B(t) \tag{46}$$

$$\theta(t+h) = \theta(t) + h\omega(t) \tag{47}$$

$$\upsilon(t+h) = \upsilon(t) + hH(x(t))^{-1}[u(t) + u_E(x(t), \upsilon(t)) - b(x(t), \upsilon(t))] \tag{48}$$

where biasing vector $b(x(t), \upsilon(t)) = C(x(t), \upsilon(t))v(t) + g(x(t))$, and h is the time-step. $T(h\omega_B)$ acts as a rotational transformer around the ω_B axis with angle $h|\omega_B|$ (see [18] and Figure 3).

$$T(h\omega_B) = \left[(\cos\psi)I_3 + (1-\cos\psi)rr^T + (\sin\psi)[r\times]\right] \tag{49}$$

where $\psi = h|\omega_B|$, $r = \omega_B/|\omega_B|$.

$H(x)$ and $b(x, \upsilon)$ can be obtained by the inverse dynamics calculation using the Newton-Euler formulation, i.e., given x, υ, and $\dot{\upsilon}$, solve for u. In fact, $H(x)$ can be calculated by solving inverse dynamics by setting x to the current state, $\dot{\upsilon} = e_j$, and ignoring centrifugal forces, Coriolis forces, gravity effects, and external forces[20]. Here, e_j means a unit vector with its j^{th} element equal to 1 and others are 0. The solution about u corresponds to the j^{th} column of H (see Eq.(7)). The biasing vector $b(x, \upsilon)$ can be also computed by setting $\dot{\upsilon} = 0$.

The inverse dynamics can be calculated by following recursive equations. The formulation is based on the algorithm in [19], but several points are different. In the proposed method, 1) there is no fixed point in the robotic system and the base-link is movable, and 2) the expression of the link-fixed coordinates is modified to deal with branching links.

The index numbers of links are introduced as shown in Figure 4 in a 14-axis biped case. Here, the link $\underline{i}$ is defined as the *inner link* of i^{th} link whose index is the smallest in all links connected to i^{th} link. Also the set of links O_i is defined as the outer links of i^{th} link whose indices are larger than $\underline{i}$ in all links connected to the i^{th} link. The examples are shown in Table 1. To compute the inverse dynamics efficiently, the

Table 1: Examples of an Inner Link and Outer Links in Figure 4 Case.

link i	1	2	7	8	14
inner link $\underline{i}$	—	1	6	1	1
outer links O_i	2,8,14,15	3	0	9	0

link-fixed coordinates shown in Figure 5 are introduced. The i^{th} coordinates are defined as ${}^0A_i = {}^0A_1\,{}^1A_2 \ldots {}^{i}A_i$ and ${}^0A_1 = A_B$, where ${}^iA_i = [{}^ix_i, {}^iy_i, {}^iz_i]$ corresponds to the i^{th} coordinates referenced to the $\underline{i}^{th}$ coordinates system. ${}^iA_i$ transforms any vector with reference to the i^{th} coordinates system to one in the $\underline{i}^{th}$ coordinates system. (Note: ${}^iA_i^{-1} = {}^iA_i^T = {}^iA_{\underline{i}}$.) In a case of the parametrization of Figure 5:

$$ {}^{\underline{i}}A_i = \begin{bmatrix} c_\phi c_\theta - s_\phi c_\alpha s_\theta & -c_\phi s_\theta - s_\phi c_\alpha c_\theta & s_\phi s_\alpha \\ s_\phi c_\theta + c_\phi c_\alpha s_\theta & -s_\phi s_\theta + c_\phi c_\alpha c_\theta & -c_\phi s_\alpha \\ s_\alpha s_\theta & s_\alpha c_\theta & c_\alpha \end{bmatrix} \tag{50} $$

where $s_\phi = \sin\phi_{i-1}$, $c_\phi = \cos\phi_{i-1}$, s_α, $= \sin\alpha_{i-1}$, c_α, $= \cos\alpha_{i-1}$, $s_\theta = \sin\theta_{i-1}$, and $c_\theta = \cos\theta_{i-1}$.

When $\dot{\upsilon}_B, \dot{\omega}_B$, ω_B, $\ddot{\Theta}_i$, $\dot{\Theta}_i$ and Θ_i are given, the angular velocity ${}^i\omega_i$, the angular acceleration ${}^i\dot{\omega}_i$, and the acceleration of the origin ${}^i\ddot{p}_i$ of i^{th} link referenced to its own link coordinates can be recurrently obtained as follows. For i=1

$$ {}^1\ddot{p}_1 = {}^1A_0\left(\dot{\upsilon}_B + g\right) \tag{51} $$

$$ {}^1\omega_1 = {}^1A_0\omega_B \tag{52} $$

$$ {}^1\dot{\omega}_1 = {}^1A_0\dot{\omega}_B \tag{53} $$

For $2 \le i \le N$

$$ {}^i\omega_i = {}^iA_{\underline{i}}\,{}^{\underline{i}}\omega_{\underline{i}} + z_0\dot{q}_{i-1} \tag{54} $$

$$ {}^i\dot{\omega}_i = {}^iA_{\underline{i}}\,{}^{\underline{i}}\omega_{\underline{i}} + z_0\ddot{\theta}_{i-1} + \left({}^iA_{\underline{i}}\omega_{\underline{i}}\right)\times z_0\dot{\theta}_{i-1} \tag{55} $$

$$ {}^i\ddot{p}_i = {}^iA_{\underline{i}}\left[{}^{\underline{i}}\omega_{\underline{i}}\times{}^ip_i^* + {}^{\underline{i}}\omega_{\underline{i}}\times\left({}^{\underline{i}}\omega_{\underline{i}}\times{}^ip_i^*\right) + {}^{\underline{i}}\ddot{p}_{\underline{i}}\right] \tag{56} $$

Thus the acceleration of the center of mass $\ddot{r}_i$, the total force F_i, and the total moment N_i, of the i^{th} link can be calculated as follows. For $1 \le i \le N$

$$ {}^i\ddot{r}_i = {}^i\dot{\omega}_i\times{}^is_i + {}^i\omega_i\times\left({}^i\omega_i\times{}^is_i\right) + {}^i\ddot{p}_i \tag{57} $$

$$ {}^iF_i = {}^im_i\,{}^i\ddot{r}_i \tag{58} $$

$$ {}^iN_i = {}^iJ_i\,{}^i\dot{\omega}_i + {}^i\omega_i\times\left({}^iJ_i\,{}^i\omega_i\right) \tag{59} $$

Here, p_i^* denotes p_i - $p_{\underline{i}}$ which is calculated as ${}^ip_i^* = [a_{i-1}\cos\phi_{i-1}, a_{i-1}\sin\phi_{i-1}, d_{i-1}]^T$. z_i denotes the direction of the joint i-1, and s_i denotes the center of mass with respect to the origin of link i coordinates (see Figure 5).

The gravity effect g is considered in Eq. (51).

Then, f_i and n_i, the force and moment exerted on link i by inner link $\underline{i}$ can be calculated as follows. For $1 \le i \le N$

$$ {}^if_i = {}^iF_i + \sum_{j\in O_i}{}^jA_j\,{}^jf_j + {}^iA_0\sum_{j\in M_i}{}^0f_{Ej} \tag{60} $$

$$ {}^in_i = {}^iN_i + \sum_{j\in O_i}\left[{}^jA_j\,{}^jn_j + {}^jp_j^*\times\left({}^jA_j\,{}^jf_j\right)\right] + {}^is_i\times{}^iF_i - \sum_{j\in M_i}\left[{}^jc_j\times\left({}^iA_0\,{}^0f_{Ej}\right)\right] \tag{61} $$

where f_{Ej} is the j^{th} external force. M_i is a set of index numbers of external forces which are imposed on link i. c_j is the position vector of the j^{th} contact point with respect to the origin of its own link-fixed coordinates as shown in Figure 6.

As a result, the solution of the inverse dynamics $u^T = [f^T_B, n^T_B, \tau^T]$ given x, υ, and $\dot{\upsilon}$ is obtained as follows, where f_B and

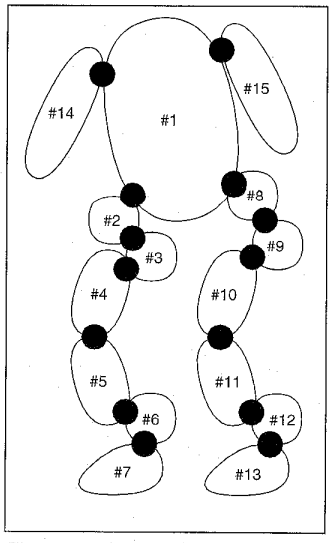

Figure 4. Indices of Links.

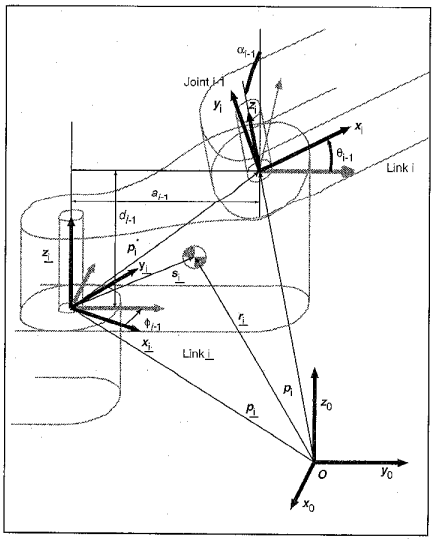

Figure 5. Coordinates and Parameters of Links.

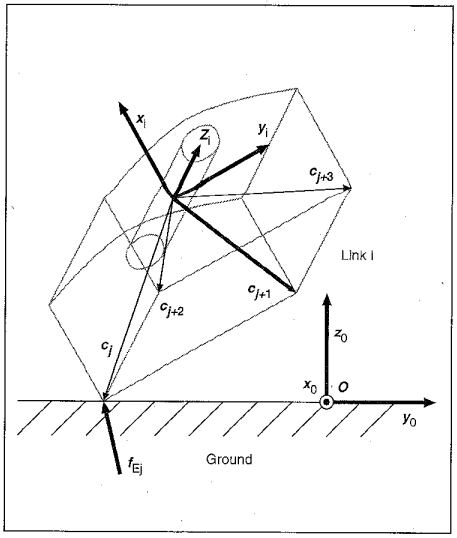

Figure 6. Contact Points.

n_B are the force and the moment exerted on the origin of the base link, respectively, and τ_i is the torque on the i^{th} joint. For $1 \le i \le N-1$

$$\tau_i = {}^{i+1}\boldsymbol{n}_{i+1}^T \boldsymbol{z}_0 - D_i \dot{q}_i \tag{62}$$

For $i = 1$

$$\boldsymbol{f}_B = {}^0\boldsymbol{A}_1 \, {}^1\boldsymbol{f}_1 \tag{63}$$

$$\boldsymbol{n}_B = {}^0\boldsymbol{A}_1 \, {}^1\boldsymbol{n}_1 \tag{64}$$

where D_i is the viscous damping coefficient of joint i.

Constrained Force

In order to support the biped robot on the ground, the appropriate reactive forces from the ground should be determined at each time step in the simulation. In general, springs and dampers models at the contact points are introduced as collision models. This simulation model, however, requires a shorter time step than the mechanical system itself does. Therefore we introduce a collision model based on a mathematical program, which is the extension of the plastic collision model[21] and can deal with the three dimensional contact and arbitrary repulsion between plasticity and elasticity. In addition, the motion with continuous collision behaves as an exact ideal constrained motion.

In general, the external force on the generalized coordinates $\boldsymbol{u}_E$ in Eq.(7) is expressed by all external forces on the contact points as follows.

$$\boldsymbol{u}_E = \sum_{i \in M_A} \boldsymbol{K}_i \boldsymbol{f}_{Ei} = \begin{bmatrix} \boldsymbol{K}_x \boldsymbol{K}_y \boldsymbol{K}_z \end{bmatrix} \begin{bmatrix} \boldsymbol{f}_{Ex} \\ \boldsymbol{f}_{Ey} \\ \boldsymbol{f}_{Ez} \end{bmatrix} = \boldsymbol{K} \boldsymbol{f}_E \tag{65}$$

where M_A represents a set of index numbers of active contact points. f_{Ex}, and f_{Ey} consist of tangent components of all active contact forces. Also f_{Ez} consists of normal components of all active contact forces. K_x, K_y, and K_z, correspond to those transformers. The dimensions of K and f_E depend on the number of the contact points, which is time-variant. In advance, K can be obtained by solving the inverse dynamics mentioned above by setting x to the current state, $f_E = e_j$, $\dot{\upsilon} = 0$, and ignoring gravity, centrifugal, and Coriolis effects.

When the external impulsive force Δf ($= f_E \, \Delta t$) is imposed on the system in Eq.(7), the following equation is realized:

$$H(\upsilon_+ - \upsilon_-) = \Delta f_b + K \Delta f \tag{66}$$

where υ_+ and υ_- denote the velocity after the collision and before the collision, respectively. Δf_b denotes the uncontrollable impulse force, i.e., $\Delta f_b \approx [u - c(x, \upsilon_-)\upsilon_- - g(x)]\Delta t$. Thus, the kinetic energy after the collision can be calculated as follows,

$$\begin{aligned} \frac{1}{2}\upsilon_+^T \boldsymbol{H} \upsilon_+ = {} & \frac{1}{2}\upsilon_-^T \boldsymbol{H} \upsilon_- + \frac{1}{2}\Delta \boldsymbol{f}^T \boldsymbol{K}^T \boldsymbol{H}^{-1} \boldsymbol{K} \Delta \boldsymbol{f} \\ & + \left(\upsilon_- + \boldsymbol{H}^{-1} \Delta \boldsymbol{f}_b\right)^T \boldsymbol{K} \Delta \boldsymbol{f} + \frac{1}{2} \Delta \boldsymbol{f}_b^T \boldsymbol{H}^{-1} \Delta \boldsymbol{f}_b \end{aligned} \tag{67}$$

The plastic collision is defined as the energy minimization with given conditions[21] which yields a quadratic programming (QP) problem. The model is expanded to the following problem to deal with three dimensional contact and arbitrary repulsion between plasticity and elasticity.

$$\underset{\Delta \boldsymbol{f}}{\text{minimize}} \quad \frac{1}{2}\Delta \boldsymbol{f}^T \boldsymbol{Q}_1 \Delta \boldsymbol{f} + \boldsymbol{q}_1^T \Delta \boldsymbol{f} \tag{68}$$

$$\text{subject to} \quad \Delta f_{zi} \ge 0 \text{ and } \sqrt{\Delta f_{xi}^2 + \Delta f_{yi}^2} \le \mu \Delta f_{zi} \tag{69}$$

where

$$\boldsymbol{Q}_1 = \boldsymbol{K}^T \boldsymbol{H}^{-1} \boldsymbol{K} \tag{70}$$

$$q_1 = K^T \left(\upsilon_- + H^{-1} \Delta f_b\right) + \begin{bmatrix} 0 \\ 0 \\ \lambda K_z^T \end{bmatrix} \upsilon_- \tag{71}$$

and λ represents a repulsion coefficient which is arbitrarily set within $0 \le \lambda \le 1$.

The problem is equivalent to

$$\underset{\Delta f_\theta}{\text{minimize}} \quad \text{the optimal value of sub-problem(72),(73)}$$

$$\underset{\Delta f_r, \Delta f_z}{\text{minimize}} \quad \frac{1}{2}\begin{bmatrix} \Delta \boldsymbol{f}_r \\ \Delta \boldsymbol{f}_z \end{bmatrix}^T \boldsymbol{Q}_2 \begin{bmatrix} \Delta \boldsymbol{f}_r \\ \Delta \boldsymbol{f}_z \end{bmatrix} + \boldsymbol{q}_2^T \begin{bmatrix} \Delta \boldsymbol{f}_r \\ \Delta \boldsymbol{f}_z \end{bmatrix} \tag{72}$$

$$\text{subject to} \quad \Delta f_{zi} \ge 0 \text{ and } \left|\Delta f_{ri}\right| \le \mu \Delta f_{zi} \tag{73}$$

where

$$\boldsymbol{Q}_2 = \begin{bmatrix} \boldsymbol{K}_r^T \\ \boldsymbol{K}_z^T \end{bmatrix} \boldsymbol{H}^{-1} \begin{bmatrix} \boldsymbol{K}_r & \boldsymbol{K}_z \end{bmatrix} \tag{74}$$

$$\boldsymbol{q}_2 = \begin{bmatrix} \boldsymbol{K}_r^T \\ \boldsymbol{K}_z^T \end{bmatrix} \left(\upsilon_- + \boldsymbol{H}^{-1} \Delta \boldsymbol{f}_b\right) + \begin{bmatrix} 0 \\ \lambda \boldsymbol{K}_z^T \end{bmatrix} \upsilon_- \tag{75}$$

$$\Delta f_{ri} = \sqrt{\Delta f_{xi}^2 + \Delta f_{yi}^2} \tag{76}$$

$$\Delta f_{\theta i} = \arctan \Delta f_{yi} / \Delta f_{xi} \tag{77}$$

$$\boldsymbol{K}_r = \boldsymbol{K}_x \cos \Delta \boldsymbol{f}_\theta + \boldsymbol{K}_y \sin \Delta \boldsymbol{f}_\theta \tag{78}$$

The constraints of the sub-problem become linear, so that the problem can be solved by non-constraint optimization algorithms (for example the quasi Newton method), including the quadratic programming sub-problem.

The solution of the problem satisfies Kuhn-Tucker's necessary and sufficient conditions as follows:

$$\mu \Delta f_{ri}^* \ge \left|\Delta f_{xi}^*\right| \tag{79}$$

$$\Delta f_{ri}^* \boldsymbol{k}_{ri}^T \upsilon_+ \le 0 \tag{80}$$

$$\left(\mu \Delta f_{zi}^* - \left|\Delta f_{ri}^*\right|\right) \boldsymbol{k}_{ri}^T \upsilon_+ = 0 \tag{81}$$

$$\Delta f_{zi}^* \ge 0 \tag{82}$$

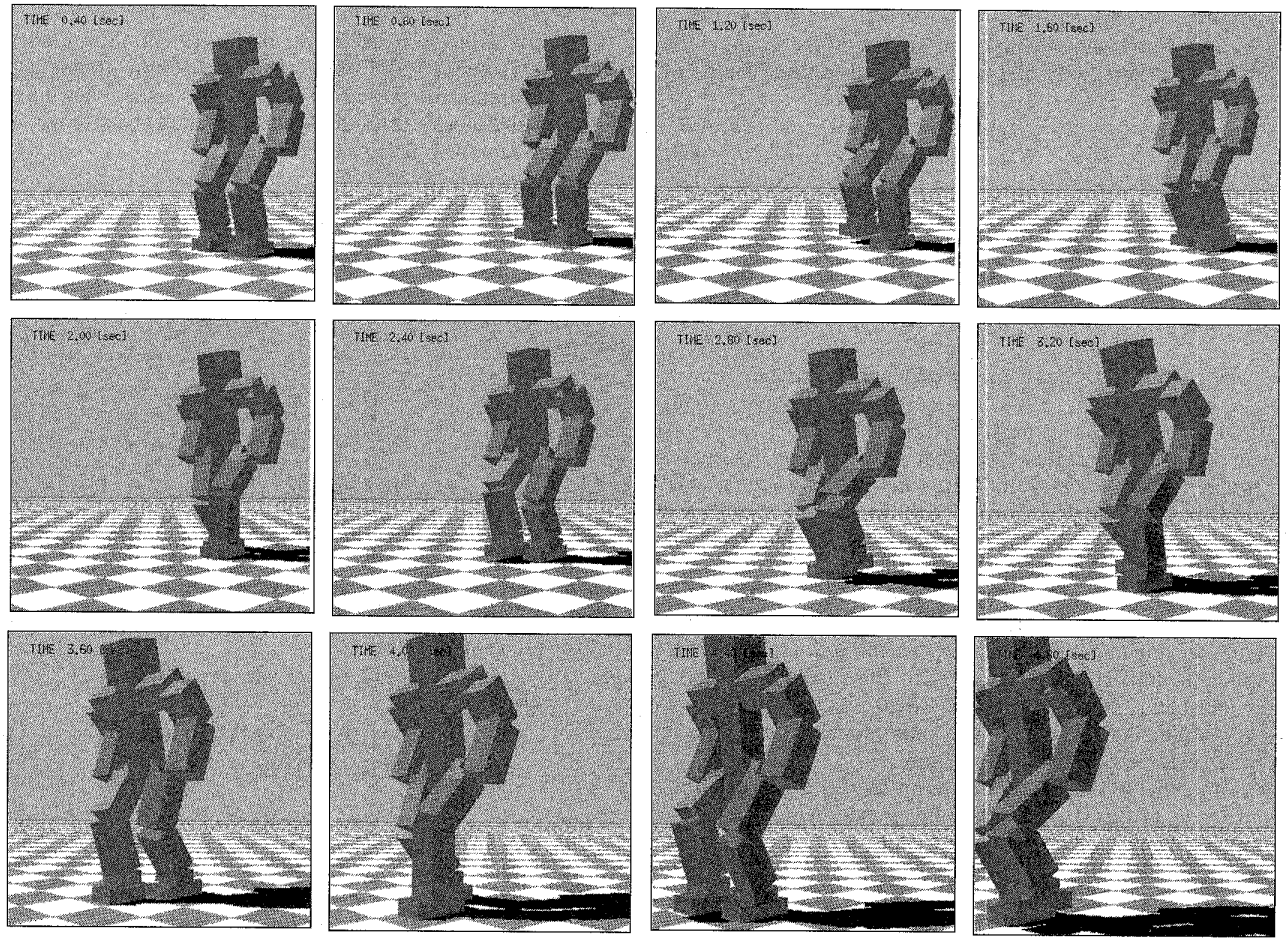

Figure 7. Snapshots of Biped Walking Simulation. (More details can be found on the Web, http://www.kawalab.dnj.ynu.ac.jp/)

$$\boldsymbol{k}_{zi}^T \upsilon_+ + \lambda \boldsymbol{k}_{zi}^T \upsilon_- \geq 0 \tag{83}$$

$$\begin{cases} \Delta f_{zi}^* \left(\boldsymbol{k}_{zi}^T \upsilon_+ + \lambda \boldsymbol{k}_{zi}^T \upsilon_- \right) = 0 & \text{if} \left| \Delta f_{ri}^+ \right| < \mu \Delta f_{zi}^* \\ \boldsymbol{k}_{zi}^T \upsilon_+ + \lambda \boldsymbol{k}_{zi}^T \upsilon_- \geq \mu \left| \boldsymbol{k}_{ri}^T \upsilon_+ \right| & \text{if} \left| \Delta f_{ri}^* \right| = \mu \Delta f_{zi}^* \end{cases} \tag{84}$$

where k_{ri} and k_{zi} denote the i^{th} row of the matrices K_r and K_z, respectively.

Conditions (79) to (81) are related to the tangent motion. Here $k_{ri}{}^T \upsilon_+$ corresponds to the tangent velocity after the collision due to the principle of the virtual work.??? Specifically, Eq.(81) means that the friction condition is activated ($|\Delta f_r^{i*}| = \mu \Delta f^*_{zi}$) if the contact point slips. If the friction condition is not activated ($|\Delta f_{ri}^*| < \mu \Delta f_{zi}^*$) the tangent velocity at the contact point becomes zero. Eq.(83) shows that the method realizes arbitrary repulsion between plasticity and elasticity. The motion with the proposed collision behaves as an exact ideal constrained motion.

SIMULATION RESULTS

The proposed control system is applied to a 20-axis human-type biped robot and is tested by a precise 3D dynamic simulator. The parameters of the robot are shown in Table 2. The control parameters are set as follows: The walking velocity: 0.25 [m/s], the walking period: 0.5 [sec/step], the double support period: 0.05 [sec], and the characteristic polynomial: $(z - 0.3)^3$.

The QP is solved by the algorithm in [22].

Snapshots of the simulation are shown in Figure 7. The initial movement of COM is completed between [0, 1]. After that, the walking motion starts. Figure 8 shows the trajectory of the zero moment point (ZMP). Figure 9 shows the response

Table 2: Parameters of Biped Robot.

Parts	Size[m]	Weight[kg]
all	0.99	28.744
head	$0.14 \times 0.14 \times 0.14 (d \times w \times h)$	2.744
arm	0.3	3.5
body	0.4	8
thigh	0.2	2
shin	0.2	2
foot	$0.2 \times 0.1 (d \times w)$	1.5

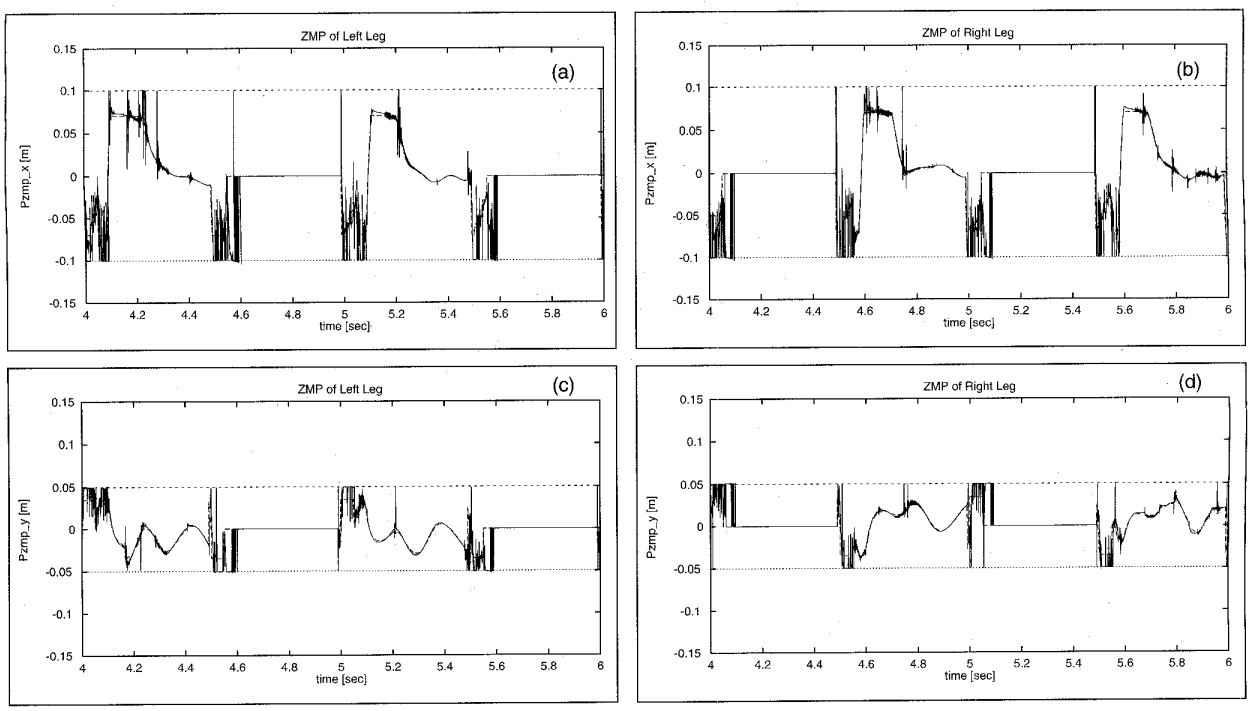

Figure 8. Trajectory of Zero Moment Point.

of COM with the reference trajectory, in which the tracking error converges to zero. From the magnified figures (c) and (d), the COM follows the inverted pendulum model even during the stepping period.

The walking motion becomes more robust when the arm swing motion compensates the yaw axis moment [17].

CONCLUSIONS

In this paper the following hierarchical control system has been proposed: 1) a posture controller which considers the physical constraints of the reactive force/torque on the foot by quadratic programming; 2) a real-time COM tracking controller by the foot placement with a discrete inverted pendulum model; 3) a three-dimensional dynamic simulation scheme with precise contact with the environment.

When the proposed control system is applied to a 20-axis simulation model, stable biped locomotion with a velocity 0.25 m/sec and a stepping time 0.5 sec/step is realized.

REFERENCES

[1] S. Kajita, T. Yamaura, and A. Kobayashi. Dynamic Walking Control of a Biped Robot Along a Potential Energy Conserving Orbit. *IEEE Trans. on Robotics and Automation*, vol. 8, no. 4, pp. 431-438, 1992.

[2] J. Furusho and A. Sano. Sensor-Based Control of a Nine-Link Biped. *Int. J. Robotics Research*, vol. 9, no. 2, pp. 83-98, 1990.

[3] J. Yamaguchi, A. Takanishi, and I. Kato. Development of a Biped Walking Robot Compensating for Three-Axis Moment by Trunk Motion. *J. Robotics Society of Japan*, vol. 11, no. 4, pp. 581-586, 1993 (in Japanese).

[4] M.H. Raibert, *Legged Robots That Balance*, Cambridge, MA, MIT Press, 1986.

[5]A. Kun and W.T. Miller, III. Adaptive Dynamic Balance of a Biped Robot using Neural Networks. *Proc. IEEE Int. Conf. on Robotics and Automation*, pp. 240-245, 1996.

[6] J.K. Hodgins. Three-Dimensional Human Running. *Proc. IEEE Int. Conf. on Robotics and Automation*, pp. 3271-3276, 1996.

[7] J. Yamaguchi, N. Kinoshita, A. Takanishi, and I. Kato. Development of a Dynamic Biped Walking System for Humanoid—Development of a Biped Walking Robot Adapting to the Human's Living Floor . *Proc. IEEE Int. Conf. on Robotics and Automation*, pp. 232-239, 1996.

[8] S. Kajita and K. Tani. Adaptive Gait Control of a Biped Robot based on Realtime Sensing of the Ground Profile. *Proc. IEEE Int. Conf. on Robotics and Automation*, pp. 570-577, 1996.

[9] H. Minakata and Y. Hori. Development of Biped Bike Prototype "Ostrich-I&II." *Proc. Asian Control Conference*, vol. 3, pp. 319-322, 1997.

[10] A.W. Salatian, K.Y. Yi, and Y.F. Zheng. Reinforcement Learning for a Biped Robot to Climb Sloping Surfaces. *J. Robotic Systems*, vol. 14, no. 4, pp. 283-296, 1997.

[11] T. Fukuda, Y. Komata, and T. Arakawa. Stabilization Control of Biped Locomotion Robot based Learning with GAs having Self-adaptive Mutation and Recurrent Neural Networks. *Proc. IEEE Int. Conf. on Robotics and Automation*, pp. 217-222, 1997.

[12] J. Pratt, P. Dilworth, and G. Pratt. Virtual Model Control of a Bipedal Walking Robot. *Proc. IEEE Int. Conf. on Robotics and Automation*, pp. 193-198, 1997.

[13] Y. Fujimoto and A. Kawamura. Three-Dimensional Digital Simulation and Autonomous Walking Control for Eight-Axis Biped Robot. *Proc. IEEE Int. Conf. on Robotics and Automation*, pp. 2877-2884, 1995.

[14] Y. Fujimoto and A. Kawamura. An Inertia Fluctuation Insensitive Robust Control of Robot Manipulators Based on a Combination of Inertia Torque Computation Filter and H. Control. *Rans. of Institute of Electrical Engineers of Japan*, vol. 117-D, no. 4, pp. 493-500, 1997 (in Japanese).

[15] Y. Fujimoto and A. Kawamura. Proposal of Biped Walking Control Based on Robust Hybrid Position/Force Control. *Proc. IEEE Int. Conf. on Robotics and Automation*, pp. 2724-2730, 1996.

[16] Y. Fujimoto and A. Kawamura. Biped Walking Control with Optimal Foot Force Distribution by Quadratic Programming. *Proc. IEEEIASME Int. Conf. on Advanced Intelligent Mechatronics*, CD-ROM, 1997.

[17] Y. Fujimoto and A. Kawamura. Robust Control of Biped Walking Robot with Yaw Moment Compensation by Arm Motion. *Proc. Asian*

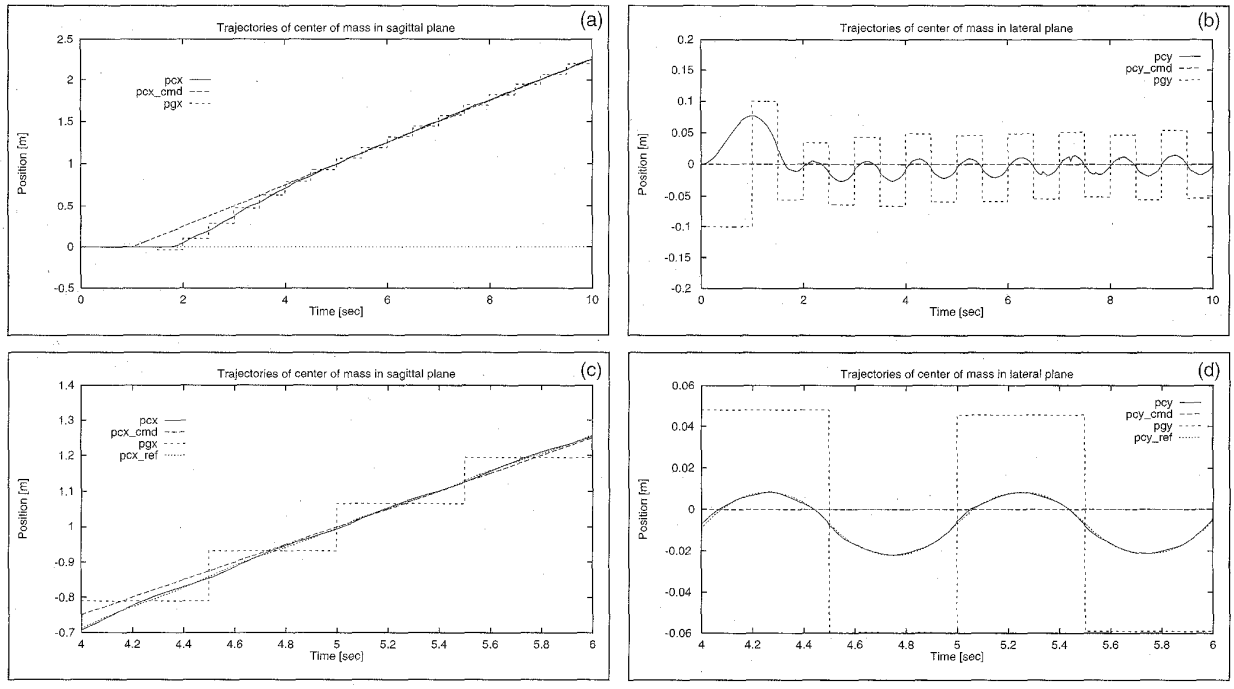

Figure 9. Trajectory of Center of Mass of the Robot.

Control Conference, vol. 3, pp. 327-330, 1997.

[18] B. Nobel. *Applied Linear Algebra*, Prentice-Hall, Englewood Cliffs, N.J., 1969.

[19] J.Y.S. Luh, M.W. Walker, and R.P.C. Paul. On-line Computational Scheme for Mechanical Manipulators. *ASME J. Dynamic Systems, Measurement, Control*, vol. 102, pp. 69-76, 1980.

[20] M.W. Walker and D.E. Orin. Efficient Dynamic Computer Simulation of Robotic Mechanisms. *ASME J. Dynamic Systems, Measurement, Control*, vol. 104, pp. 205-211, 1982.

[21] P. Lötstedt. Numerical Simulation of Time-Dependent Contact and Friction Problems in Rigid Body Mechanics. *SIAM J. Scientific and Statistical Computing*, vol. 5, no. 2, pp. 370-393, 1984.

[22] R.W. Cottle and G.B. Dantzig. Complementary Pivot Theory of Mathematical Programming. *Linear Algebra and Its Applications*, vol. 1, pp. 103-125, 1968.

Yasutaka Fujimoto (S'93-M'98) was born in Kanagawa, Japan in 1971. He received B.S., M.S., and Ph.D degrees in electrical engineering from Yokohama National University, Yokohama, Japan, in 1993, 1995, and 1998, respectively. He was a Research Fellow of the Japan Society for the Promotion of Science from 1995 to 1998.

In 1998 he joined the department of electrical engineering at Keio University, Yokohama, Japan as a research associate.

His research interests are motion control, biped robots, and intelligent systems. Dr. Fujimoto is a member of the IEE of Japan and the Robotics Society of Japan.

Atsuo Kawamura (S'77-M'81-SM'96) was born in Yamaguchi Prefecture, Japan, in 1953. He received the B.S., M.S., and Ph.D. degrees in electrical engineering from the University of Tokyo, Tokyo, Japan, in 1976, 1978, and 1981, respectively.

In 1981 he joined the Department of Electrical and Computer Engineering at the University of Missouri-Columbia as a postdoctoral fellow, and was an assistant professor there from 1983 through 1986. In 1986 he joined the department of elecrical and computer engineering at Yokohama National University, Yokohama, Japan as an associate professor, and became a professor in 1996. He has been the department head from 1997 to 1998. His interests are in power electronics, digital control, ultrasonic actuators, electric vehicles, robotics, and so on. He is a recipient of IEEE IAS Transactions Prize Paper Award in 1988, and IEE of Japan Transactions Prize Paper Award in 1996. He was the conference chairperson of IEEE/IAS and IEEJ/IAS joint Power Conversion Conference (PCC-Yokohama) in 1993. He is an associate editor of *IEEE Transactions on Power Electronics*. He will serve as the technical program chairman of Power Electronics Specialist Conference in 1998 (PESC'98).

Dr. Kawamura is a member of the IEE of Japan, IEEE, Robotics Society of Japan, the Institute of Electronics, Information and Communication Engineers, and the Society of Instrument and Control Engineering.